Chipless Dielectric Constant Sensor for Structural Health Testing

Antonio Lazaro, *Senior Member, IEEE*, Ramon Villarino, Filippo Costa*, Member IEEE,* Simone Genovesi, *Member IEEE*, Antonio Gentile, Luca Buoncristiani, David Girbau, *Senior Member, IEEE*

¹

Abstract— **A low-cost chipless RFID sensor tag to determine the dielectric properties of materials is presented. The sensor is based on a depolarizing dipole resonator loaded with printed capacitors whose capacitance depends on the permittivity of the material located on contact with the tag. The permittivity is obtained from the shift of the resonance frequency. The resonator is tested both individually as well as placed on a periodic arrangement so as to form a frequency selective structure (FSS) to increase the cross polar radar cross section, thus facilitating the tag detection. The proposed structure and measurement procedure is particularly suitable for the characterization of civil materials as a non-destructive testing (NDT).**

*Index Terms—***Chipless RFID, Frequency Selective Surfaces (FSS), non-destructive testing (NDT), concrete, permittivity sensor.**

I. INTRODUCTION

Chipless radio identification (RFID) tags are passive transponders that do not uses a microchip. Chipless RFID technology has emerged during last years in the literature. The main research efforts have been oriented to increase the number of bits that the electromagnetic structure can encode [1-3] or developing low cost printing techniques ~~for manufacturing~~ to manufacture low cost tags. However, this technology has also been proposed as a sensor [4-11]. In these cases, due to the limited number of sensors within the read range of the tag, it is not necessary a large number of bits to perform the identification and conventional methods such as barcodes, QR codes, or NFC tags can be used. In this work, a chipless RFID tag is proposed as relative permittivity sensor that can be used for Non-destructive testing (NDT). Non-destructive testing of materials is an important issue in civil structures [12], [13]. It is especially important in the case of concrete, since its structural properties depend on the mixture of compounds. A wrong mixture could cause a structure to collapse. For these reasons, samples of the materials are periodically inspected in the laboratory. However, in situ

methods and long-term non-destructive testing (NDT) of the civil structures are highly desirable. Several works have already proposed different wireless sensors for structural health monitoring [13-18]. A wireless sensor network is often used to collect the data from distributed sensors [13], [15]. A fiber optic link used for monitoring the strain of civil infrastructures at long distances is described in [13]. In the recent years, the RFID technology has been introduced for construction supply chain control [19]. In the line of this work, some passive RFID sensors have been proposed. A passive water-content sensor based on the detuning of a low-frequency resonator has been proposed in [14]. A similar concept is used for corrosion detection in [15] or dielectric permittivity measurements [16]. The detuning of the UHF RFID antenna is also used to sense dielectric constant in [17]. A UHF RFID integrated circuit that contains a temperature sensor has been proposed for monitoring the temperature during concrete maturation [20].

Due to the absence of a battery and any electronic component, the proposed tag is cheaper than the active ones and it is suitable for harsh environments. The tag consists of a bent dipole over a ground plane loaded with capacitors whose capacitance depends on the relative permittivity of the material that is on contact with the tag. Therefore, its resonance frequency depends on the electrical characteristics of this material. The paper is organized as follows. Section II presents the system and the sensing principle. Section III presents the simulations of the tag. Some preliminary experimental results are presented in Section IV. Section V presents a method to calibrate the tag and the experimental results. Finally, Section VI draws the conclusions.

II. SENSING PRINCIPLE

A chipless frequency-coded tag is based on one or several resonators that produces a change in the frequency response of the Radar Cross Section (RCS). Then, the detection is based on the measurement of the resonance frequency. However, the reflections at the environment (especially large objects near the tag) are often noticeably higher than the power reflected at the tag when conventional (non depolarizing) resonators are used. This makes tags difficult to be detected in real environments, especially when attached to large elements, such as civil structures. To this end, this work uses of depolarizing tags [1], [2], [9-11]. Depolarizing tags based on resonators have been introduced in [2] and they show good performance when they are attached to lossy materials. Additionally, in this application, the reflections produced on

the wall are mainly in the incoming polarization. Therefore, the use of a depolarizing tag overcomes this drawback.

A representation of the measurement system is shown in Fig.1. The tag is remotely read using a Vector Network Analyzer (VNA) that works as a reader. The reader sends a polarized wave (e.g. using a vertical oriented Vivaldi antenna) and then sweeps the interrogation frequency in order to measure the resonance frequency of the tag that depends on the material behind it. The tag can be detected measuring the cross polar component using a cross-polarized antenna (e.g. using a horizontal oriented Vivaldi antenna) in reception. Therefore, the reception antenna filters the reflection on the wall and receives the backscattered field produced on the tag. In addition, the coupling interference between transmission and reception antennas is also minimized when using depolarizing tags.

A Frequency Selective Surface (FSS) composed of a depolarizing resonator is used as dielectric constant sensor (Fig.2). It uses four-unit cell resonators to increase the level of the reflected signal and facilitate the sensor detection. The depolarizing resonator is based on a bent dipole loaded with two capacitors etched on the ground and connected to the resonant structure through vias. Fig.3. describes the layout of the unit cell.

A model of the proposed tag is shown in Fig.3a where the distributed capacitor is modelled with its lumped equivalent. The perpendicular arms generate the depolarization of the incident wave and their length must be adequately tuned [10]. The resonance frequency can be tuned by changing the capacitor geometries. The capacitors are patterned in the ground plane in order to sense the materials attached to the tag (see the layout of Fig.3). Their capacitances depend on the slot width and the permittivity of the material. Therefore, a frequency shift in the resonance is expected as a function of the permittivity. A qualitative electrical model is shown in Fig.4.b. It consists of a section of microstrip lines with the two lumped capacitors. A simplified model for the capacitor is composed of the via inductance and the distributed capacitance.
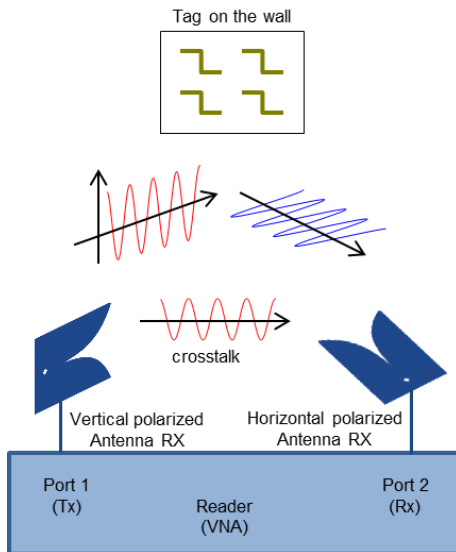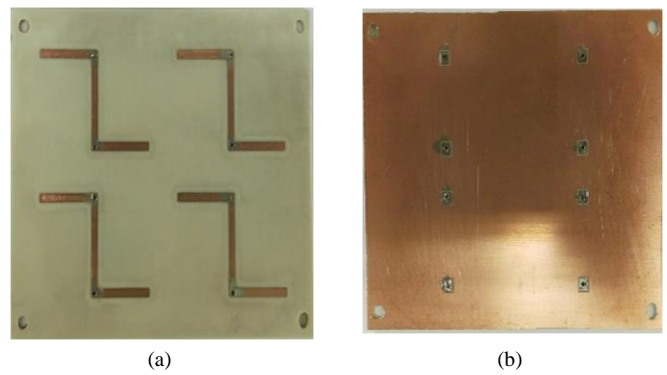

(a)　　　　　　　　　　　(b)

Fig.2. Prototype of the sensor tag composed by four unit cells. (a) Top view, (b) bottom view.
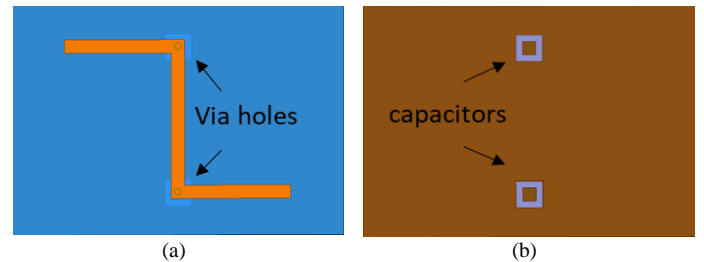

(a)　　　　　　　　　　　(b)

Fig. 3. Layout of the tag unit cell (a) top side, (b) bottom side. The via holes that connect the resonator in the top layer and the patch in the bottom layer have been marked. In the bottom, the sensing capacitor is formed by a slot ring around the small patch.
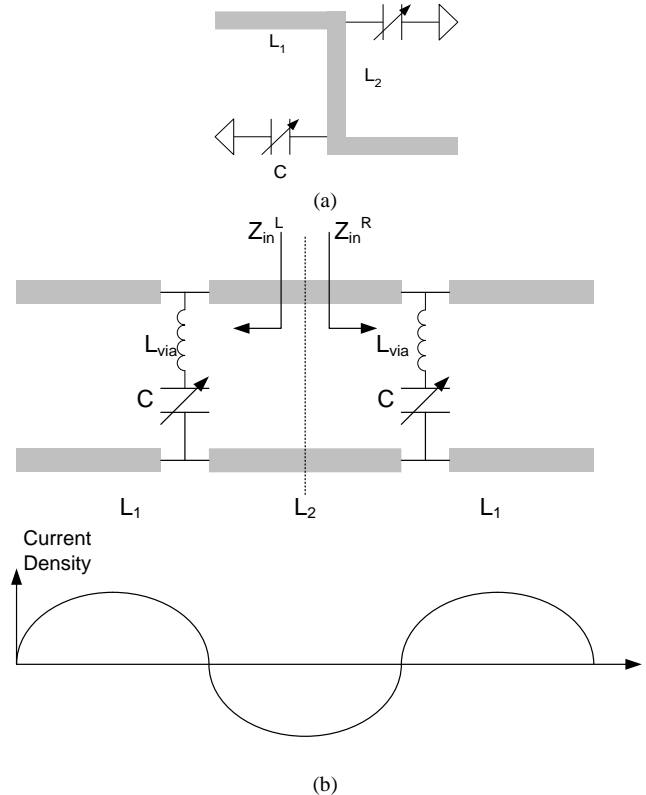

(a)

(b)

Fig. 4. Unit cell resonator (a), transmission line model and approximated current distribution (b).

Fig.1. Schema of the measurement system.

III. SIMULATIONS

In order to maximize the cross-polar component, the induced current in the lateral arms must be comparable to the current in the center of the dipole that contributes mainly to the co-polar component of the radar cross section. The current at the ends of the unit cell resonator must be zero imposed by the open circuit condition. The capacitor presents a low impedance at the resonance frequency. Therefore, a low value of current is expected at this point. An approximated current distribution along the resonator is shown in Fig.4.b. This current distribution has been verified by means of electromagnetic simulations that will be shown below. It can be expected that the 3rd resonance increases the cross-polar components. Therefore, a simplified circuit of Fig.4.b for the determination of resonance frequency can be proposed. The equivalent circuit is composed by a microstrip transmission line of length L_2 that models the section of the resonator oriented in the copolar direction (vertical direction in Fig.1-2). This line is loaded with two microstrip transmission lines of length L_1 that model the propagation in the bent lines. The sensors at the corners are modelled as capacitors whose capacitance changes with the dielectric constant of the material under the ground plane. An inductor connected in series with the capacitance between the slot ring and the ground models the inductance of the via hole that connects the strip line printed on the top layer and the small patch situated just under the line on the bottom layer (see Fig.3).

The resonance frequency can be obtained from the transverse resonance method [21]. If the middle point in the model of Fig.4.b is considered. This means that the impedance Z_{in}^R looking forward must be equal to minus the impedance Z_{in}^L looking backward, so that $Z_{in}^L + Z_{in}^R = 0$. The other resonances can be obtained applying the dual condition, $Y_{in}^L + Y_{in}^R = 0$.

The impedance from the middle point can be obtained from the input impedance of a transmission line of length $L_2/2$ and a characteristic impedance Z_0 loaded with an impedance Z_L:

$$Z_{in}^{L,R} = Z_0 \frac{Z_L + jZ_0 tan(\beta L_2/2)}{Z_0 + jZ_L tan(\beta L_2/2)} \quad (1)$$

Where Z_L is the parallel combination impedance of the capacitance C in series with inductance L_{via} and the open circuit transmission line of length L_1:

$$Z_L = \frac{1}{\frac{1}{j\omega L_{via} + 1/(j\omega C)} + j\left(\frac{1}{Z_0}\right)tan(\beta L_1)} \quad (2)$$

Fig.5 shows the variation of the 3rd resonance frequency as function of the capacitance (C) that loads the dipole. It is numerically obtained solving the resonance condition equation using a zero-search routine (with Matlab) and it is checked using a circuit simulator (Keysight ADS). A typical inductance of 2.5 nH for the via hole is considered. It is demonstrated that, for capacitances smaller than 2.5 pF, the behavior is nearly linear, therefore it is expected to obtain a linear dependence with the permittivity of the material located behind the ground plane. Fig.6 shows the simulation of the capacitance of the slot capacitor (C) performed with Keysight Momentum) with a gap of 0.8 mm as function of the dielectric permittivity of the material behind the tag. It can be observed that the capacitance C varies linearly with the permittivity.
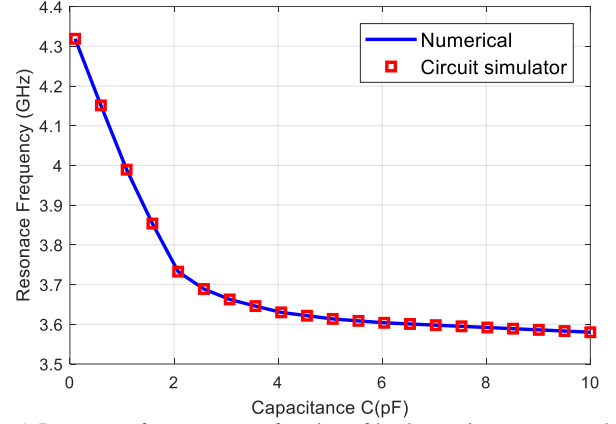

Fig.5. Resonance frequency as a function of load capacitance computed with the transmission line model (-) and the circuit simulator (□).
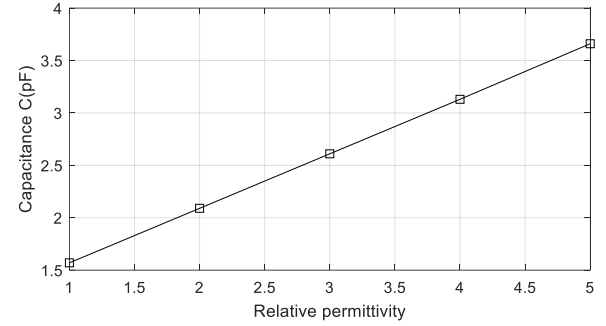

Fig.6. Simulated capacitance of the slot capacitor as function of the relative permittivity of the material.

As a proof of concept, a design at 4 GHz is performed. This frequency is selected because it matches with the peak gain of the antennas used in the experimental setup and where the maximum isolation is achieved. However, the design can be easily scaled to other frequencies by changing the length of the dipoles. The chosen lengths of dipole arms are L_1=20 mm, L_2=22 mm and the width is 2 mm. The via's hole diameter is 1 mm and the slot gap in the ground plane is 0.8 mm. The parameters have been chosen keeping a compromise between the quality factor of the resonance and the level of cross polar radar cross section. From the image electromagnetic theory, the image currents induced in the ground plane under the strips have opposite sign with respect the current in the strips. Therefore, a partial cancellation of the radiation fields is produced due to these currents. Small substrate thickness results on high quality factors but the cross polar RCS is smaller than when thicker substrates are used. The substrate used in these prototypes is Roger RO4003 with 64 mil thickness in order to facilitate tag detection. However, to derive a simple model from the slot capacitance is not straightforward. For this reason, HFSS 3D electromagnetic simulations are used to confirm the previous model. Fig.7 shows the current distribution of the unit-cell element at the frequency that maximizes the cross-polar component. The current distribution confirms the behavior predicted in Fig.4b. The high current introduced in the folded arms produces the cross-polar component of the radar cross section. Fig.8 shows HFSS simulations of the cross-polar RCS for materials located behind the tag with different permittivities (ε_r). A smooth

frequency shift, of the same order than the predicted by the transmission model, is appreciated. The width of the slot in the ground plane (see Fig.3) can be used to perform a fine tuning of the resonance frequency as it is shown in the simulations of Fig.9. In practice, this parameter is sensitive to the layout tolerance, especially if the printed board is manufactured using custom facilities. Fig.10 shows the effect of loss introduced by the material attached behind the tag. To avoid the dependence of the result with the thickness of material a 10 mm slab is considered in the simulations, since in real environments tags will be embedded on the surface of a thick material under test. The quality factor decreases, and a frequency shift is predicted. Therefore, the tag can be useful for materials with low or moderate losses, being wet samples very difficult to detect.
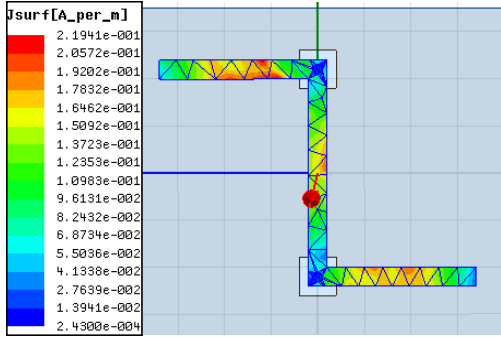

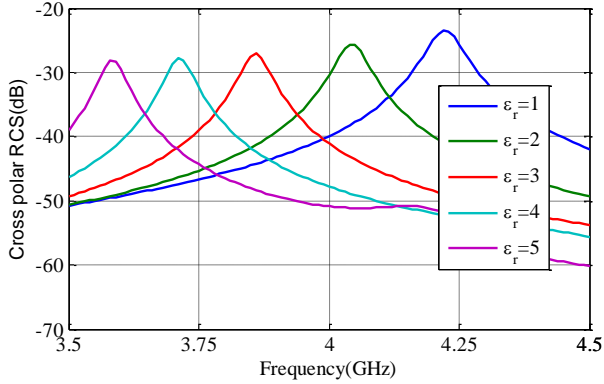Fig. 7. Current density distribution in the resonator.

Fig.8. Simulated cross-polar RCS as a function of the frequency for different permittivity of the material behind.
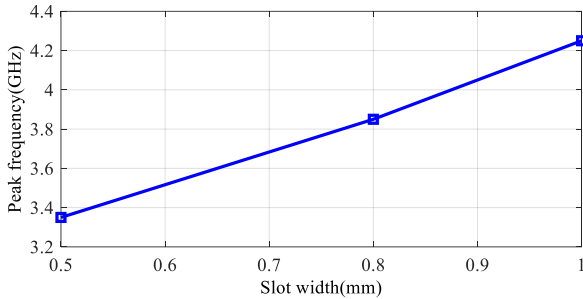

Fig. 9. Simulation of the tag response on air with respect to the slot width.
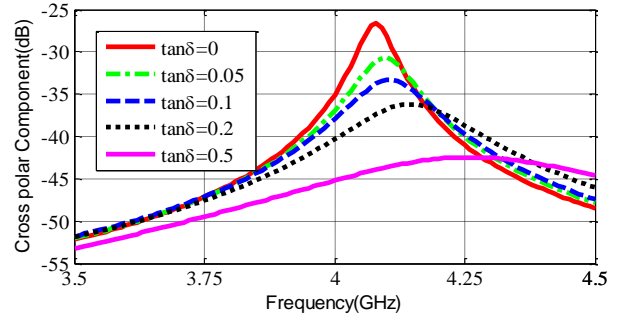

Fig. 10. Effect of material losses in the tag response.

IV. PRELIMINARY EXPERIMENTAL VALIDATION WITH BACKGROUND SUBTRACTION

In order to increase the RCS and the detectability, the manufactured tag is composed by four unit cells, as shown in Fig.2. Fig.11 reports the measurements of backscattered cross-polarized fields for different materials with known permittivity. These results will be used to calibrate the sensor. The thickness of the materials behind is larger than 10 mm to avoid dependence of the frequency shift also on the thickness. The results are obtained using the background subtraction technique that consists of subtracting the measurement of the scene without the tag from the measured parameter S_{21} in presence of the tag. The same smooth frequency shift observed in simulations are found. The resonant frequency obtained is slightly lower than in simulations due to the coupling between elements and the tolerances in the fabrication of the slot and the via holes using a custom circuit manufacturing facility. Therefore, the experimental permittivity calibration procedure may be required. Fig.12 shows the variation of the frequency peak obtained from Fig.11 as a function of the material permittivity. A linear regression is made with good agreement. This line can be used to measure the permittivity of unknown materials. An additional important parameter is the read range and the repeatability of the measurement when the distance changes. Fig.13a shows the measurement of the tag on the air as a function of the reader-to-tag distance. When the distance increases, the received level clearly decreases however the peak frequency remains constant. A read range close to 1 m is estimated, if a minimum signal-to-noise ratio of 10 dB is assumed. The read-range can be increased by adding more unit cells, at the expense of increasing the tag size as can be shown in Fig.13b. The resonance frequency of the tag with only one element (unit cell) and the FSS with 2 x 2 elements is the same but the range achieved is higher in this case compared to the one element case, 100 cm in front of 40 cm An improvement of 12 dB is obtained as it was expected due to increase of the radar cross section of the FSS that depends of N^2, where N is the number of cells [22].
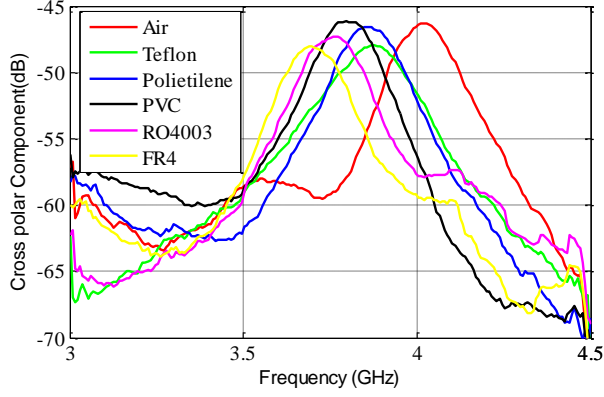
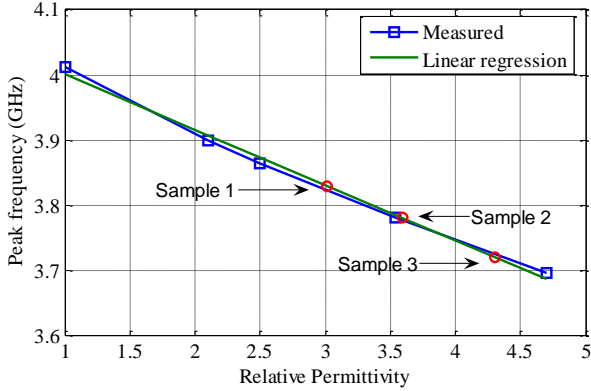Fig. 11. Measured cross-polar component after background subtraction for different materials behind the tag.

Fig.12. Measured peak frequency as a function of the permittivity of known materials (□). A linear regression is applied to measured resonances of sample materials (o).
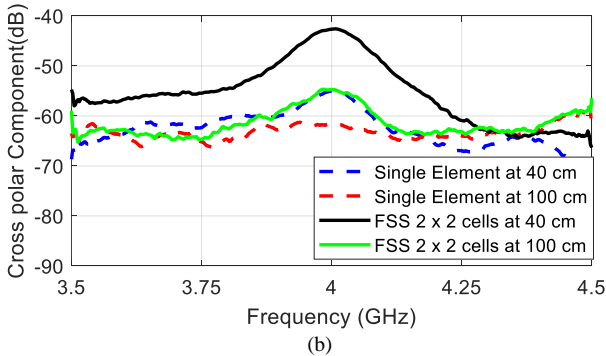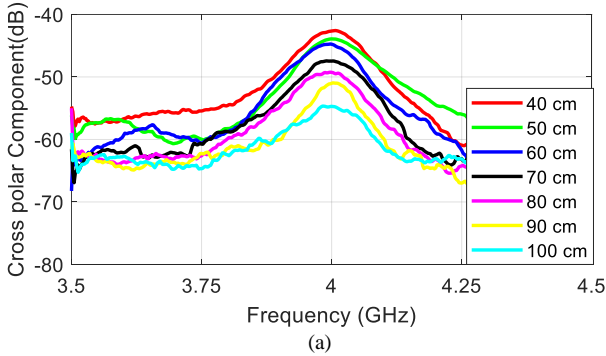

(a)

(b)

Fig. 13. (a) Measured response of the tag composed by 4 elements for different reader-to-tag distances. (b) Measured response of the tag composed by 4 elements and single element at distance of 40 cm and 100 cm

V. ON-SITE CALIBRATION TECHNIQUES

One of the main difficulties in chipless RFID technology is the S-parameters calibration needed for tag detection. Usually the background subtraction technique is used, but this approach is unpractical in most real applications, since it requires to remove the tag to measure the scene [1-3]. For long-term NDT of civil structures, the tag is inserted during the fabrication of the structure and it is periodically measured (after the sample is dry). Therefore, the tag cannot be removed to perform background subtraction. In order to solve this problem some alternatives have been investigated.

First of all, an analysis of the received signal (parameter S_{21} measured between the transmit and receive antennas) is taken into account. The measured signal can be modelled as the sum of three contributions: the tag response, $s_{tag}(t)$, the coupling interference between the antennas, $s_c(t)$, and the clutter due to the backscattered field on the surrounding objects, $s_{clutter}(t)$.

$$s(t) = s_{tag}(t) + s_c(t) + s_{clutter}(t) \qquad (3)$$

The coupling signal is due to the crosstalk between the antennas and depends on the antennas used and the distance between them. It can be considered constant with respect to the distance between the tag and reader and often it presents a much higher amplitude than the tag and the clutter. The amplitude of the tag response depends on the distance between tag and reader. The clutter response can be split in a couple of terms: one due to the objects close to the tag and the other due to the objects far from the tag. The first contribution presents higher amplitude and it often strongly depends on frequency. In case of depolarizing tags, the reflection in flat surfaces such as walls or ground is minimized because co-polar component that is filtered by the receiver antenna in cross polarization is produced. Following the model (3), the tag response can be obtained subtracting a reference measurement without tag response ($s_{ref}(t) \approx s_c(t) + s_{clutter}(t)$) to the measurement of the tag. Therefore, the reference measurement can be obtained eliminating the tag response by locating an absorbent that attenuates the reflection in both polarizations or placing a metallic plate that eliminates the reflection in the cross polar component. In both cases, it is assumed that the clutter is invariant along the measurement with the tag and the calibration with the reference. The metallic plate can be replaced by the wall or another material where the tag is attached, assuming that the distance remains invariant.

Two different practical scenarios are considered. In the first one, the read range is very small (20-30 cm), and in the second one the distance to the material under test is higher (50 cm). In all the cases, the crosstalk between antennas dominates, especially outside the resonance frequency of the tag, but it is removed using any of the previous reference measurements. In the first case, the tag response dominates over the clutter contributions, whereas in the second the clutter amplitude is dominant. For small read range (Fig.14.a), the tag can be detected easily from the raw measurement without subtracting any reference measurement because the amplitude of the backscattered field in cross polarization is higher than the other contributions, mainly in copolar components. Therefore, only one measurement is needed. However, for longer

distances (Fig.14.b) it is not possible to detect the tag from the raw measurement.

Experimental results with the tag attached on a wall of bricks in the laboratory (indoor environment) located at 20 cm and 50 cm from the antennas are shown in Figure 14.a and 14.b, respectively. Fig. 15 shows a photograph of the experiment where the tag is on contact with the wall. These figures show the raw measurement (parameter S_{21} between two cross-polarized antennas), and the signal obtained by subtracting the following reference measurements: the wall without the tag, a metallic plate (used as reference tag), an absorbent material that covers the tag and the crosstalk measurement of the antennas. A piece of Eccosorb VHP-4 with a typical reflectivity of -30 dB at the operating band with the same area of the tag and thickness of 5 cm is used as absorber. In both of the tested scenarios, the tag can be detected using a metallic plate or an absorber as background, or subtracting the crosstalk between antennas. This crosstalk measurement can be stored once and subtracted to all tag measurements. A good agreement is obtained between the three calibration procedures. As conclusion, the detection of the proposed permittivity sensor based on a FSS made of depolarizing resonators can be measured up to 50 cm.
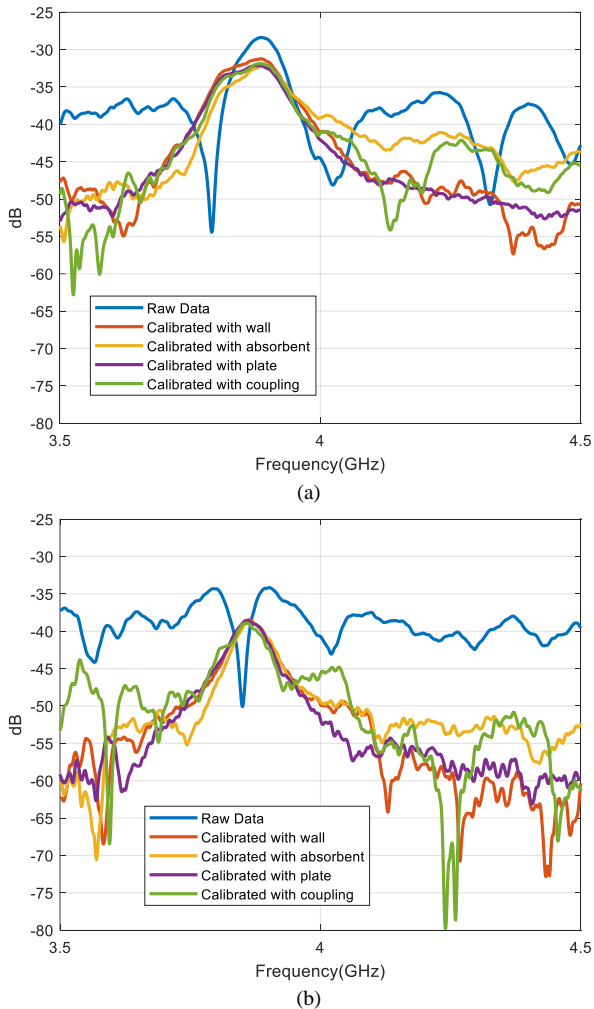

Fig.15. Photography of the experimental setup for measurement of the tag in a wall.

VI. EFFECT OF HUMIDITY AND TEMPERATURE

Finally, the measurement method is tested, in a realistic environment, with different types of walls. Sample 1 is a wall of concrete (100% concrete), sample 2 is a block of 50% concrete and 50% sand and sample 3 is a wall of bricks. In order to compare the values of permittivity obtained with the chipless sensor, the samples have also been measured with the ring resonator method [6]. In this characterization method, the permittivity is obtained from the frequency shift of the resonance frequency [23]. A ring resonator printed on 1.6 mm thick Rogers 4003 has been designed to resonate around 4 GHz (see Fig.16). The first resonance frequency can be obtained from the effective permittivity ε_{ref} given by [24]:

$$f_r = \frac{c}{2\pi R \sqrt{\varepsilon_{ref}}} \tag{4}$$

$$\varepsilon_{ref} = \frac{\varepsilon_{rs} + \varepsilon_{rmat}}{2} + \frac{\varepsilon_{rs} - \varepsilon_{rmat}}{2}\left(1 + \frac{12 W_e}{h}\right)^{-1/2} \tag{5}$$

Where R is the radius of the resonator (6.9 mm), W is the width of the line (1.85 mm), h is the thickness of the substrate (32 mil) and t is the metallization thickness (34 µm). ε_{rs} and ε_{rmat} is the relative permittivity of the substrate and the material, respectively. W_e is the effective width given by:

$$W_e = W + \frac{t}{\pi}\left(1 + ln\left(\frac{2h}{t}\right)\right) \tag{6}$$

When the material under test is located on the top of the resonator, a shift in the resonance frequency is produced due to the variation of the effective permittivity. Fig.17 shows the resonator's relative frequency shift, considering the presence and absence of a material on the top. The expressions (4)-(6) have been checked with electromagnetic simulations with Keysight Momentum. Fig.18. depicts an example of measurement, where both the frequency shift and the reduction of the quality factor due to the presence of the block of concrete are clearly visible. Table I compares the permittivity obtained using the calibration line obtained in Fig.12 and the measurement of the samples using the ring resonator method. The average difference between the two methods is 3.94%.

(a)

(b)

Fig.14. Comparison of the raw measurement of the tag on a wall at 20 cm (a) and 50 cm (b) for different calibration procedures.
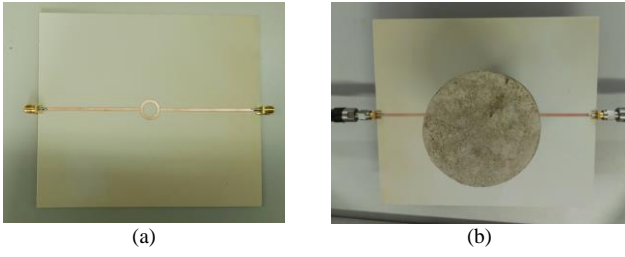
Fig.16. Photography of the unloaded ring resonator (a) and loaded with a block of concrete (b).

TABLE I
SAMPLE COMPOSITION AND PERMITTIVITY

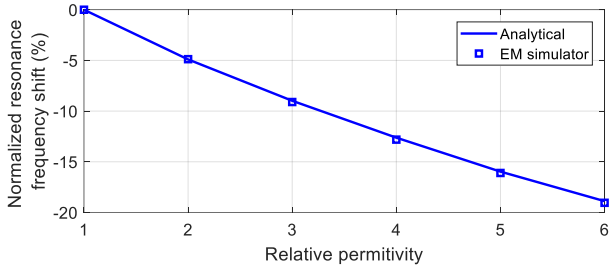| Sample	Material	Measured permittivity Chipless tag	Measured permittivity Ring resonator method	Difference (%)
1	Concrete 100%	3.56	3.51	3.55
2	Concrete 50%	3.98	4.07	3.97
3	Wall of bricks	4.31	4.24	4.30

Fig.17. Normalized frequency shift with respect the ring resonator loaded with the air as function of the material relative permittivity. Comparison between the analytical (solid line) model and EM simulations (□) with Keysight Momentum.
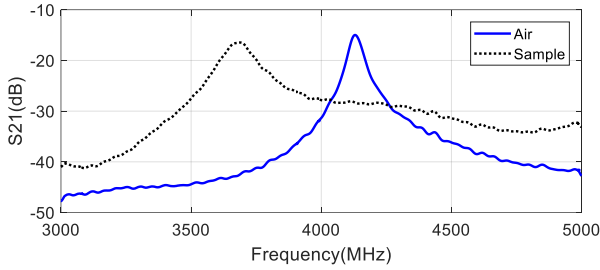

Fig.18. Measured S_{21} for the ring resonator unloaded (in air, solid line) and with a sample block of concrete (dotted line).

In order to study the influence of the moisture in the sample some experiments have been done. First, a dry concrete wall is measured. Later the wall has been wet with water and the measurement has been repeated. The results are shown in Fig.19. A shift in the measurement is depicted due to the moisture, but the peak frequency returns to the dry value when the sample tends to dry state after 1 h. The absorption of moisture by the substrate used to print the tag due to the ambient humidity can also affect the measure. In order to quantify it a ring resonator is introduced in a climatic chamber. Fig. 20 shows the variation of the permittivity of the Rogers 4003 substrate over a cycle from 0 to 100%. A variation of 0.1 in the permittivity and a recover of its initial value when substrate is dried can be observed. The reduction of the quality factor or increase of the tangent losses as

consequence of the water absorption is also observed. The result of variation in the resonance frequency of the ring resonator is 1%. It can be expected that the variation of the measurement of chipless tag will be of the same order.

The temperature can also affect the measurement of the resonance of the chipless tag. A small change in the permittivity of the substrate and the expansion of the resonator is produced. Fig. 21 compares the measurement of a tag (at approximately distance of 20 cm from the reader) on the air at 25ºC and after heating with a heat gun at 100ºC. The variation is -9.1 MHz. This variation is smaller than the bandwidth (about 100 MHz) of the measured peak. Therefore, the error can be neglected for the typical temperature measurement range.
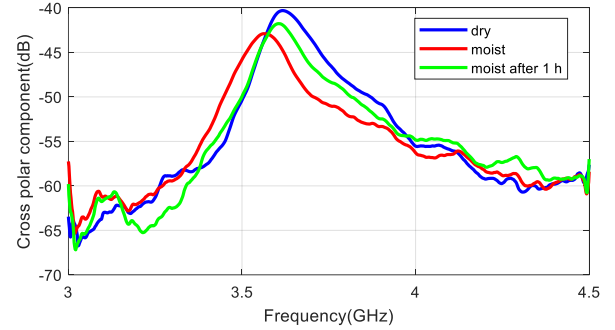

Fig.19. Comparison of a measurement of a wall of concrete as function of the moist degree.
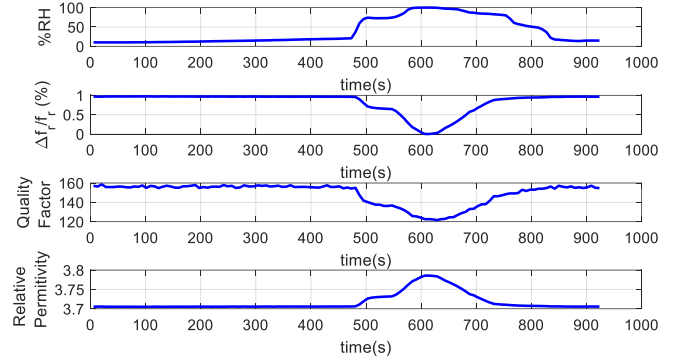

Fig.20. Variation of the resonance frequency, quality factor and relative permittivity of a ring resonator made with Rogers 4003 as function of the time when the relative humidity change (top).
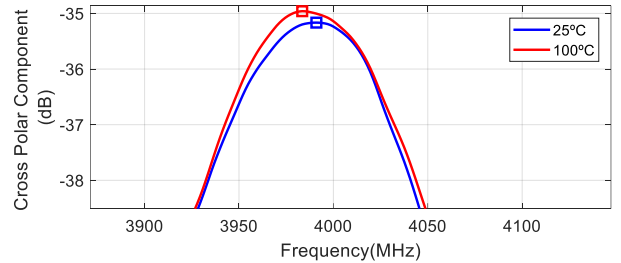

Fig.21. Comparison of a tag measurement at 25 ºC and 100 ºC.

VII. DETECTION WITH LOW-COST SDR READER

One important drawback of chipless technology over well-established commercial RFID technologies (HF or UHF

RFID) is the lack of commercial readers. Therefore, the measurements are often performed using VNA available at laboratories. However, some proof of concept prototypes has been proposed in the literature. A prototype based on a VCO and a phase/gain detector (AD8302) between 1.9 GHz and 2.5 GHz is reported in [25]. Software defined radio (SDR) N210 USRP platform based on powerful FPGA is used as reader in [26]. Another reader based on time-domain UWB sampler is presented in [27], [28]. Additionally, low-cost VNA can be found in the market that can replace benchtop VNA for field measurements. Experimental results of section V.A shows that for small distances, scalar measurements can achieve good precision because the scattered field by the tag is high enough to neglect the coupling. Therefore, these results open the door to use simplified low-cost readers such as spectrum analyzers with tracking generator option or low-cost receivers as described next. As a proof of concept, a low-cost reader based on a popular low-cost SDR receiver (RTL-SDR based on RTL2832U chipset) is used. As the frequency band of the RTL2832U is up to 2 GHz, a down-converter based on a mixer (LRMS30J from Minicircuits) is used. The local oscillator for the mixer and the transmitter can be implemented using a phase-lock-loop (PLL) synthesizer (from IDM Instruments). The received signal at fixed IF (1.5 GHz) is sampled by the RTL-SDR receiver. The data is transferred to the computer by USB. After filtering the data, the Hilbert transform is applied to the sampled signal obtaining both amplitude and phase information. The reader is powered by USB, therefore a portable reader can be implemented. Fig.22 shows the block diagram and a photography of the prototype. Fig. 23 shows a short range (20 cm) typical tag measurement which achieves good agreement with that obtained with the VNA.
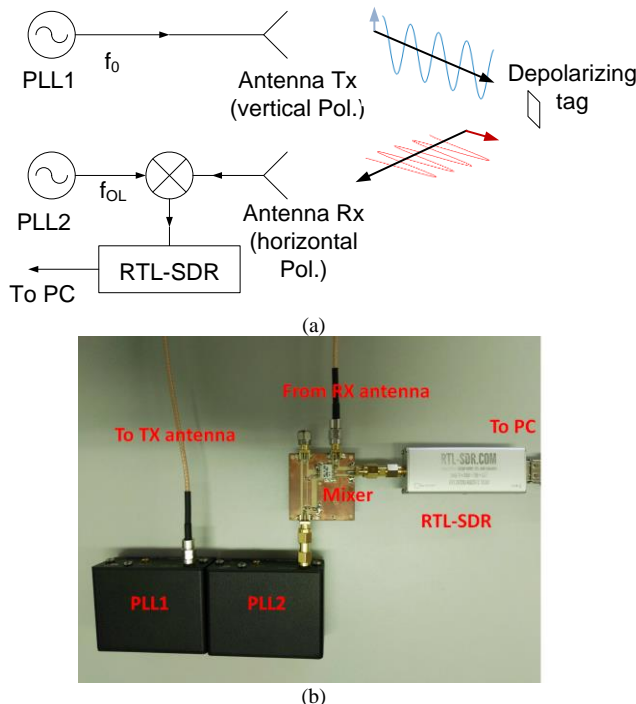

Fig.22. (a) Block diagram and photography (b) of the reader based on a low-cost SDR receiver.
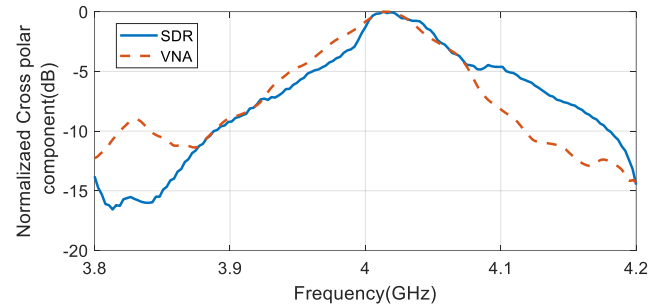

Fig.23. Comparison of a measurement as function of the frequency performed with the SDR based reader and with VNA.

VIII. CONCLUSION

A novel cross-polarized chipless sensor based on a depolarizing dipole loaded with capacitors is proposed as permittivity sensor for long-term non-destructive testing of structures. A simple model based on a loaded transmission line is presented. Simulated and experimental results show a nearly-linear dependence of the resonance frequency of the tag with the permittivity, which permits the calibration of the sensor. The tag has been tested in realistic scenarios and different procedures to detect the sensor on large civil structures are proposed, which do not require tag removal, as an alternative to background subtraction. For small distances the tag can be detected from the raw measurement without subtracting any background subtraction. However, for higher distances, the tag can be detected subtracting the crosstalk measurement or using a reference tag composed by a metallic plate in front the tag or an absorbent. The influence of temperature, moist and ambient humidity is empirically analyzed. Finally, the feasibility of low-cost based on SDR receiver has been demonstrated for short ranges.

REFERENCES

[1] S.Preradovic, I. Balbin, N.C. Karmakar, G.F. Swiegers, "Multiresonator-based chipless RFID system for low-cost item tracking", *IEEE Transactions on Microwave Theory and Techniques*, Vol.57, No.5, pp.1411-1419, 2009.

[2] A.Vena, E.Perret, S.Tedjini, "Chipless RFID tag using hybrid coding technique," *IEEE Transactions on Microwave Theory and Techniques*, Vol.59, No.12, pp.3356-3364, 2011.

[3] A. Lazaro, A. Ramos, D. Girbau and R. Villarino, "Chipless UWB RFID Tag Detection Using Continuous Wavelet Transform," *IEEE Antennas and Wireless Propagation Letters,* Vol. 10, pp. 520-523, 2011

[4] D.Girbau,A.Lazaro, R.Villarino, "Passive wireless permittivity sensor based on frequency-coded chipless RFID tags," *IEEE Microwave Symposium Digest (MTT)*, pp. 1-3, 2012.

[5] D. Girbau, Á. Ramos, A. Lazaro, S. Rima, and R. Villarino, "Passive Wireless Temperature Sensor Based on Time-Coded UWB Chipless RFID Tags," IEEE *Trans. Microw. Theory Tech.*, Vol. 60, No.11, pp. 3623–3632, 2012.

[6] A.Ramos, D.Girbau, A.Lazaro, R.Villarino, "Wireless concrete mixture composition sensor based on time-coded UWB RFID," *IEEE Microwave and Wireless Components Letters*, Vol.25, No.10, pp.681-683, 2015.

[7] Y. Feng, L. Xie, Q. Chen and L. R. Zheng, "Low-Cost Printed Chipless RFID Humidity Sensor Tag for Intelligent Packaging," *IEEE Sensors Journal,* Vol. 15, No. 6, pp. 3201-3208, June 2015

[8] A.Lazaro, A.Ramos, D.Girbau, R.Villarino, "Signal Processing Techniques for Chipless UWB RFID Thermal Threshold Detector Detection," *IEEE Antennas and Wireless Propagation Letters*, Vol.15, pp.618-621, 2016.

[9]   E.Perret, "Permittivity characterization based on Radar Cross measurements," *URSI International Symposium on Electromagnetic Theory (EMTS)*, pp. 457-460, 2016.

[10] M. Borgese, F. Costa, S. Genovesi, A. Monorchio, and G. Manara, "Multi-frequency polarizarition converter with enhanced angular robustness," in *2016 IEEE International Symposium on Antennas and Propagation (APSURSI)*, pp. 669–670, 2016.

[11] M.Borgese, F.Dicandia, F.Costa, S.Genovesi, G.Manara, "An Inkjet Printed Chipless RFID Sensor for Wireless Humidity Monitoring," *IEEE Sensors Journal*, Vol.17, No.15, pp.4699-4707, 2017.

[12] J. P. Lynch, "An overview of wireless structural health monitoring for civil structures," *Phil. Trans. R. Soc. A*, Vol. 365, No. 1851, pp. 345-372, 2007.

[13] S. Liehr et al., "Polymer Optical Fiber Sensors for Distributed Strain Measurement and Application in Structural Health Monitoring," *IEEE Sensors Journal,* Vol. 9, No. 11, pp. 1330-1338, 2009.

[14] J. B. Ong, Z. You, J. Mills-Beale, E. L. Tan, B. D. Pereles and K. G. Ong, "A Wireless, Passive Embedded Sensor for Real-Time Monitoring of Water Content in Civil Engineering Materials," *IEEE Sensors Journal*, Vol. 8, No. 12, pp. 2053-2058, 2008.

[15] Q. Ling, Z. Tian, Y. Yin and Y. Li, "Localized Structural Health Monitoring Using Energy-Efficient Wireless Sensor Networks," *IEEE Sensors Journal,* Vol. 9, No. 11, pp. 1596-1604, 2009.

[16] M. Alamin, G.Y. Tian, A.Andrews, P.Jackson, "Corrosion detection using low-frequency RFID technology," *Insight-Non-Destructive Testing and Condition Monitoring*, Vol.54, No.2, pp.72-75, 2012.

[17] R. Suwalak, C. Phongcharoenpanich, D. Torrungrueng, and M. Krairiksh, "Determination of Dielectric Property of Construction Material Products Using a Novel RFID Sensor," *Progress in Electromagnetics Research*, Vol. 130, pp. 601-617, 2014.

[18] S. Higashi and T. Fukusako, "A sensor antenna for non-destructive testing," *IEEE Conference on Antenna Measurements & Applications (CAMA)*, Chiang Mai, pp. 1-3, 2015.

[19] Q.Shi, X.Ding, J.Zuo, G.Zillante, "Mobile Internet based construction supply chain management: A critical review," *Automation in Construction*, vol. 72, part 2, pp. 143-154, 2016.

[20] S. Manzari, T. Musa, M. Randazzo, Z. Rinaldi, A. Meda and G. Marrocco, "A passive temperature radio-sensor for concrete maturation monitoring," 2014 IEEE RFID Technology and Applications Conference (RFID-TA), Tampere, 2014, pp. 121-126.

[21] D.M.Pozar, Microwave engineering, John Wiley & Sons, 2nd Ed. New York, 1998.

[22] F. Costa, S. Genovesi, and A. Monorchio, "A Chipless RFID Based on Multiresonant High-Impedance Surfaces," *IEEE Transactions on Microwave Theory and Techniques*, vol. 61, no. 1, pp. 146–153, Jan. 2013.

[23] F. Costa *et al*., "Progress in green chipless RFID sensors," *2017 11th European Conference on Antennas and Propagation (EUCAP)*, Paris, 2017, pp. 3917-3921.

[24] I.J. Bahl and D. K. Trivedi, "A Designer's Guide to Microstrip Line", Microwaves, May 1977, pp. 174-182.

[25] S. Preradovic and N. C. Karmakar, "Design of short range chipless RFID reader prototype," *2009 International Conference on Intelligent Sensors, Sensor Networks and Information Processing (ISSNIP)*, Melbourne, VIC, 2009, pp. 307-312.

[26] A.El-Awamry, M. Khaliel, A. Fawky, M. El-Hadidy and T. Kaiser, "Novel notch modulation algorithm for enhancing the chipless RFID tags coding capacity," *2015 IEEE International Conference on RFID (RFID)*, San Diego, CA, 2015, pp. 25-31.

[27] M. Garbati, R. Siragusa, E. Perret and C. Halopé, "Low cost low sampling noise UWB Chipless RFID reader," *2015 IEEE MTT-S International Microwave Symposium*, Phoenix, AZ, 2015, pp. 1-4.

[28] R. V. Koswatta and N. C. Karmakar, "A Novel Reader Architecture Based on UWB Chirp Signal Interrogation for Multiresonator-Based Chipless RFID Tag Reading," in *IEEE Transactions on Microwave Theory and Techniques*, vol. 60, no. 9, pp. 2925-2933, Sept. 2012.